



Precatalyst or dosing-device? The $[\text{Pd}_2\{\mu\text{-(C}_6\text{H}_4\text{) PPh}_2\}_2\{\mu\text{-O}_2\text{C(C}_6\text{H}_5\text{)}\}_2]$ complex anchored on a carboxypolystyrene polymer as an effective supplier of palladium catalytically active nanoparticles for the Suzuki-Miyaura reaction



M. Ángeles Úbeda^{a,1}, Pedro Amorós^{b,1}, Juan F. Sánchez-Royo^b, Jamal El Haskouri^b, M. Dolores Marcos^c, Francisco Pérez-Pla^{b,*,1}

^aDepartament de Química Inorgànica, Universitat de València, Dr. Moliner 50, 46100 Burjassot, València, Spain

^bInstitut de Ciència dels Materials (ICMUV), c/Catedrático José Beltrán 2, 46980 Paterna, València, Spain

^cCentro de Reconocimiento Molecular y Desarrollo Tecnológico (IDM), Unidad Mixta Universitat Politècnica de València - Universitat de València. Departamento de Química, Universitat Politècnica de València, Camino de Vera s/n, 46022 València, Spain

ARTICLE INFO

Article history:

Received 30 July 2019

Revised 23 September 2019

Accepted 9 October 2019

Keywords:

Suzuki-Miyaura

Palladium nanoparticles

Carboxypolystyrene polymer

Heterogeneous homogeneous catalysis

Kinetic study

STEM-HAADF

HRTEM

XRD

SEM

ABSTRACT

A new catalyst has been synthesized from the precursor $[\text{Pd}_2\{\mu\text{-(C}_6\text{H}_4\text{) PPh}_2\}_2\{\mu\text{-O}_2\text{C(C}_6\text{H}_5\text{)}\}_2]$ immobilized on a carboxypolystyrene polymer that exhibits an excellent dispersion of the Pd (II) centers, reusability, and catalytic activity in front of phenyl bromides. The activity of this new material was studied in detail for the Suzuki-Miyaura reaction and compared to that of Pd nanoparticles (NPs) supported on UVM-7 (a mesoporous silica), and Pd NPs stabilized with polyvinylpyrrolidone. The homogeneous/heterogeneous character of the catalytic process was determined from the results of the hot-filtration, centrifugation, poisoning, three phases tests, and from differential sensitivity kinetic assays. Changes in the palladium oxidation state, and the size and morphology of the Pd NPs formed during several reusing catalytic cycles were determined by XPS, and by SEM and STEM-HAADF respectively. Kinetic and structural analyses concluded that the new material behaved as a supplier of active Pd(0) NPs to the Suzuki-Miyaura catalytic cycle, which was determined to be driven mainly by the palladium fraction present in solution.

© 2019 Elsevier Inc. All rights reserved.

1. Introduction

Palladium catalyzed reactions are involved in many of the processes used in organic synthesis [1–3]. In this context, the palladium carbon-carbon coupling reactions have allowed to synthesized valuable natural products, complex organic molecules, pharmaceuticals, agricultural chemicals, or advanced materials [4–7].

Palladium complexes have used as precatalysts in homogeneous catalysis with high reactivity and selectivity although they show the difficulty of recycling for reuse or contamination of the products obtained. With the idea in mind of designing sustainable and economic processes, the use of heterogeneous systems was proposed and developed quickly. Since 1970s many palladium

compounds have been immobilized in organic, inorganic, or hybrid supports [8–10].

Polystyrene (PS) and styrene/divinylbenzene (PS-DVB) copolymers are the most popular organic polymeric insoluble supports because of their stability, mechanical robustness, low cost, highlighting their facile functionalization [11–16]. Among the different strategies used in the complex immobilization: covalent bonding, ion-pair formation, encapsulation, or entrapment, the most used corresponds to the covalent binding through functional groups of the modified polymer since this procedure can limit the leaching of the supported complex.

The palladium immobilized precatalyst undoubtedly become nanoparticles (NPs) in the first cycle [16]. The sigmoidal reaction kinetics very often observed in cross-coupling reactions are assigned to this transformation that contributes the catalytically active Pd(0) species [17]. Although some authors consider that the immobilization of homogeneous complexes on an expensive support that ends up giving NPs, adds complexity to the catalytic

* Corresponding author.

E-mail address: francisco.perez@uv.es (F. Pérez-Pla).

¹ All these authors have contributed equally.

system and none have used for the industry [18], nowadays it is relevant to deepen into the knowledge of which species are active in the heterogeneous catalysis as well as if the catalytic process is truly homogeneous or heterogeneous [19–22], since it is the starting point for the design of more selective and efficient catalysts.

The “cocktail-of-species” model is currently being considered [16,23]. Recently Polynski and Anakinov [17] have demonstrated through a detailed computational study, the validity of this model for palladium catalysts in ArX oxidative-addition-dependent reactions. Regardless of the palladium precatalyst, three types of species were considered: Pd NPs, Pd molecular species (depending on reaction type, for example $X[PhPdX]_{1-2}X^{2-}$) and inactive Pd.

Being the catalysis a kinetic phenomenon it should be considered that kinetic data can provide information about all these questions. In a previous work, we have studied the activity of a Pd NPs-UVM-7 catalyst synthesized by immobilizing the precursor (**3**, see Scheme 1) on UVM-7 silica [24], and subsequent reduction of Pd(II) with hydrazine [25]. The prepared material was relevant because of the high dispersion, small size, and high activity of the silica supported Pd NPs. The kinetic study suggested, however, that most of the catalytic action fell on the solubilized Pd fraction, which resulted in a high activity in the Suzuki-Miyaura (SM) reaction but causing a rapid deactivation of the material by the aggregation of the solubilized Pd in the liquid phase. The question that arises is if the catalyst activity can be maintained, but increasing its reusability simultaneously. With the aim to answer the question, the new Pd(II) carboxy-polystyrene supported material described below was prepared, and its activity compared to that of the previously silica supported catalyst. Kinetic studies were also applied and the transformation of the Pd(II) complex immobilized were also studied.

2. Experimental

2.1. Reagents and materials

Commercially available 4-substituted phenylhalides, biphenyl compounds, and the carboxypolystyrene resin (1% cross-linked functionalized in 0.5–1.5 mmol/g) were supplied by Aldrich. HPLC grade solvents CH_2Cl_2 (Baker), CH_3OH (Scharlau), ethanol (Scharlau, 96% v/v extrapure), and CH_3CN (Baker) were used without further purification. Complexes $[Pd_4(\mu-Br)_4\{\mu-(C_6H_4)PPh_2\}_4]$ [26] (**1**), and $[Pd_2\{\mu-(C_6H_4)PPh_2\}_2\{\mu-O_2C(C_6H_5)\}_2]$ [27] (**2** (see Scheme 3)) were prepared according to the method described in the literature.

2.2. Instruments

Characterization of Materials. The palladium and phosphorus contents were determined by energy dispersive X-ray spectroscopy (EDX) analysis using a scanning electron microscope (Phillips - SEM-XL 30). For electron microscopy analyses, the samples were dispersed in ethanol and placed onto a carbon coated copper microgrid and left to dry before observation.

The TEM and HRTEM microstructural characterizations were carried out using a JEOL JEM-1010 instrument operating at 100 kV and equipped with a CCD camera and a Tecnai G2 F20(FI) instrument, respectively. STEM-HAADF images were acquired on a JEOL-2100F microscope operated at 200 kV. Powder X-ray diffraction (XRD) was carried out using a Bruker D8 Advance diffractometer with monochromatic $Cu K\alpha$ source operated at 40 kV and 40 mA. Patterns were collected in steps of 0.02° (2θ) over the angular range $1-10.0^\circ$ (2θ), with an acquisition time of 25 s per step. Additionally, XRD patterns were recorded over a wider angular range, $10-80^\circ$, (2θ) to determine the presence of segregated crystalline phases.

Surface area values were calculated from nitrogen adsorption-desorption iso-therms ($-196^\circ C$) recorded on a Micromeritics ASAP-2020 automated analyzer.

X-ray photoelectron spectra (XPS) were recorded with an Omicron spectrometer equipped with an EA-125 hemispherical electron multichannel analyzer and an unmonochromatized $Mg K\alpha$ X-ray source having radiation energy of 1253.6 eV. XPS spectra of the precatalyst and the catalysts after several cycles were recorded in order to follow the evolution.

FTIR spectra of the polymeric support and precatalyst were characterized before and after the cross-coupling reaction using an Agilent Cary 630 FTIR spectrophotometer.

Kinetic studies. HPLC measurements were carried out using a chromatograph (Jasco) equipped with an analog-digital converter (Jasco LC-Net II), quaternary gradient pump (PU-2089), diode array detector (MD-2018), column oven (Jasco co-2065 Plus), manual injector (Reodhyn 720i, loop 5 μL), and a 150×4.6 mm C-18 Kromasil column (stationary phase 5 μm C-18 functionalized silica particles from Scharlau). 1H NMR spectra were recorded at 298 K with a Bruker 400 and a 500 AMX spectrometers. Samples were dissolved in $CDCl_3$ or CD_2Cl_2 . Chemical shifts (δ in ppm) were referred to $Si(CH_3)_4$.

2.3. Synthesis of the Pd(II) precatalyst (**4**)

Partial deprotonation of the carboxypolystyrene polymer. Carboxypolystyrene resin (1 g) was suspended in a solution of KOH (56.1 mg, 1 mmol) in CH_3OH (5 mL). The suspension was vigorously stirred for 1 h, filtered, and the solid washed with $H_2O:CH_3OH$ (2:1 v/v), CH_3OH , and CH_2Cl_2 . The white solid was allowed to air dry.

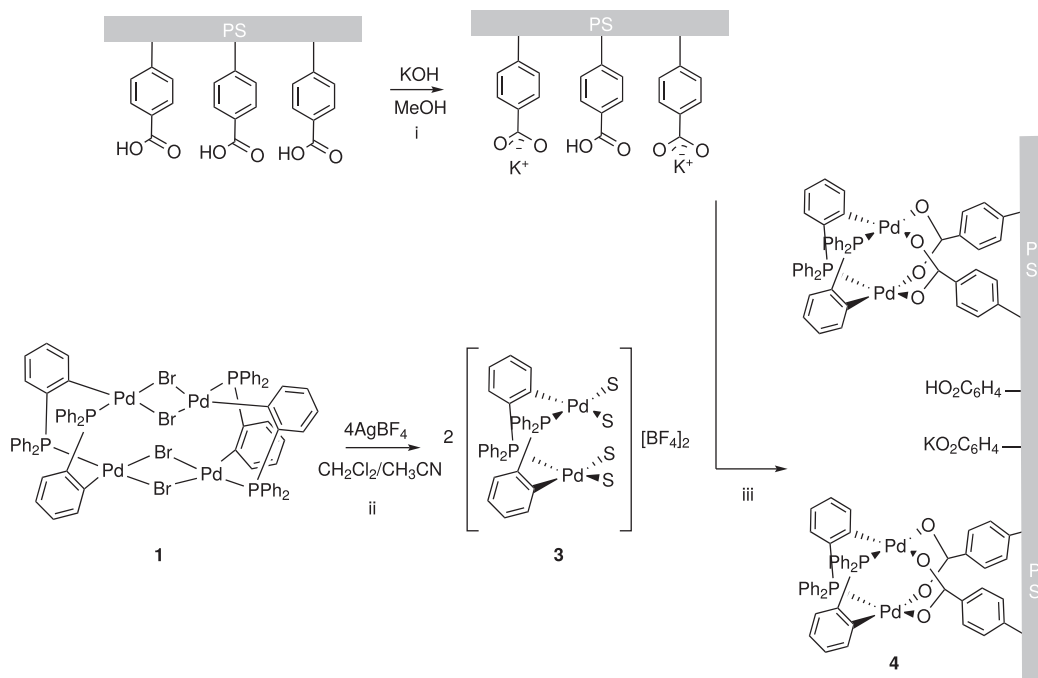
Immobilization of complex (1**) on the carboxypolystyrene polymer.** Complex (**1**) (50 mg, 0.028 mmol) was suspended in a mixture of CH_2Cl_2 (3 mL) and CH_3CN (0.15 mL) in a Schlenk tube under nitrogen atmosphere. $AgBF_4$ was added (23 mg, 0.118 mmol), the tube covered with an aluminum foil, and the suspension stirred for 45 min at room temperature. The resulting yellowish solution together with the $AgBr$ precipitate formed were exposed to the sunlight to reduce $Ag(I)$ to $Ag(0)$. In a second Schlenk tube, the deprotonated carboxypolystyrene resin (1 g) was suspended in CH_2Cl_2 (5 mL) and, handling carefully the vacuum, the content of the first tube was transferred to the second one under nitrogen atmosphere through a flexible pipe equipped with a filter. The new suspension was stirred for 1 h, and the yellow solid, the precatalyst $[Pd_2\{\mu-(C_6H_4)PPh_2\}_2\{\mu-O_2C(C_6H_4-PS)\}_2]$ (**4**), was filtered, washed with CH_2Cl_2 and allowed to air dry.

2.4. Synthesis of the stabilized Pd NPs

H_2PdCl_4 was freshly prepared by reaction of $PdCl_2$ (22 mg, 0.124 mmol) and HCl (1.3 mL, 0.2 M). A solution of polyvinylpyrrolidone (PVP, 211 mg) in deionized water (50 mL) was added to the yellow reaction mixture and stirred for 30 min. Then, $NaBH_4$ (15 mL, 0.053 M) ($Pd:NaBH_4$ 1:6.4) was added slowly under vigorous magnetic stirring, resulting in the immediate formation of brown $Pd(0)$ NPs. The suspension was evaporated to dryness and the solid was subsequently dispersed by sonication in 50 mL of a mixture of $H_2O/ethanol$ (1:4 v/v). These NPs were prepared for comparative purposes dealing with the catalytic experiments.

2.5. HPLC calibration and analysis procedures

HPLC standards were prepared by diluting with ethanol stock solutions containing the 4-substituted phenyl halide (10^{-2} M)



Scheme 1. Synthesis procedure of the precatalyst (4). (i) Partial deprotonation of the carboxylic groups of the polymer. (ii) Synthesis of the cationic complex (3). (iii) Immobilization of the Pd(II) on the carboxypolystyrene polymer.

and its reaction product ($0.5 - 1.0 \times 10^{-2}$ M) in ethanol. The chromatographic separation of the reaction samples was carried out passing as the eluent a solution of CH₃CN and H₂O (0.1% v/v in HCl) in a ratio 70:30 v/v through a C-18 reverse phase column thermostated at 40 °C at a rate flow of 1.0 mL/min.

2.6. General procedure for the kinetic study of the Suzuki-Miyaura reaction

In a typical experiment, the 4-substituted phenyl halide (XC₆H₄R X = I, Br; R = NO₂, COCH₃, H, OCH₃, CH₃; 0.5 mmol), phenylboronic acid (0.75 mmol), K₂CO₃ (0.75 mmol), and ethanol (50 mL, 96% v/v) were introduced into a 2-neck flask equipped with a cooler and a thermostat jacket attached to a water bath. After heating at 60 °C, a sample of 0.3 mL was taken (the blank) and the precatalyst added (typically in 1 mol % with respect to the 4-substituted phenyl halide, 45 mg, [Pd] = 1.0×10^{-4} M). The progress of the reaction was monitored taking aliquots (0.3 mL) at regular time intervals. After sampling, aliquots were poured into vials containing ethanol (96%, 2 mL) and HCl (0.15 M, 0.1 mL) as the quencher. The resulting solution was filtered with a 0.02 μm pore size microfilter (from Whatman), and portions of 5 μL of the filtrate were analyzed according to the HPLC procedure described above.

2.7. Reusing of the catalyst by centrifugation/washing procedure

The study of the precatalyst reusing was carried out following the general procedure, using 4-iodoanisole as the substrate. The first cycle was completed after 120 min, then the catalyst was separated by centrifugation and washed with ethanol to remove the reactant and product residues. The recovered solid was dried at 70 °C for 24 h and used in the next cycle. The addition of reagents in each cycle was that specified in the general procedure except for K₂CO₃, the mass of which was reduced by half (0.375 mmol) from the second cycle, as it was not completely removed during washing. The process was carried out several times reaching a total of

6 cycles. The experiment was repeated doubling the analytical concentration of Pd.

2.8. Investigation of the homogeneous vs. heterogeneous nature of catalysis

Hot filtration test. 4-iodoanisole (118.0 mg, 0.504 mmol), phenylboronic acid (92.8 mg, 0.761 mmol), K₂CO₃ (104.0 mg, 0.753 mmol), and the precatalyst (47.1 mg, ≈1% in Pd relative to the substrate) were added to the reactor and allowed to react in ethanol (50 mL) at 60 °C for 15 min. By this time, a sample of the reaction mixture (12 mL) was taken, filtered, and the supernatant poured on a second flask maintained at the work temperature, allowing the reaction to continue for 24 h. The samples taken before and after the filtration were analyzed by the HPLC technique described above.

Centrifugation test. 4-iodoanisole (117.2 mg, 0.501 mmol), phenylboronic acid (93.0 mg, 0.763 mmol), K₂CO₃ (104.0 mg, 0.752 mmol), and the precatalyst (47.0 mg, ≈1% in Pd relative to the substrate) were allowed to react in ethanol (50 mL) at 60 °C. A portion of the reactive mixture (20 mL) was removed after 14 min. of reaction, centrifuged, and the supernatant liquid (12 mL) poured into another flask maintained at the work temperature. The progress of the reaction in both flasks was monitored by HPLC.

Catalyst poisoning. 4-iodoanisole (112.3 mg, 0.480 mg), phenylboronic acid (99.1 mg, 0.812 mmol), K₂CO₃ (109.6 mg, 0.790 mmol), and the precatalyst (47.0 mg, ≈1% in Pd relative to the substrate) were allowed to react in ethanol (50 mL) at 60 °C. QuadraPure TU (500 mg) was added after 36 min. of reaction. The progress of the reaction was monitored by HPLC.

Three phases test. The three phases test was carried out following the procedure published by Crudden et al. [28], Kantman et al. [29], and Gruber-Woelfler [30]. Amino functionalized silica gel (BrPhCONH₂-SiO₂) was synthesized according to the method described in the literature. 4-iodoanisole (93.3 mg, 0.400 mmol), phenylboronic acid (104.1 mg, 0.854 mmol), K₂CO₃ (117.1 mg,

0.847 mmol), and ethanol (50 mL) were introduced in a reaction flask, and the mixture heated up to 60 °C. After blank extraction, the precatalyst (46.2 mg, ≈1% in Pd) and functionalized BrPhCONH₂-SiO₂ silica gel (500 mg) were introduced into the reactor. After 60 min. of reaction the solid was separated by filtration, and washed with ethanol and CH₂Cl₂. The solid was hydrolyzed following the procedure described in the literature. The 4-bromobenzoic acid and [1,1'-biphenyl]-4-carboxylic acid obtained were analyzed by ¹H NMR spectroscopy.

2.9. Schmidt's analysis of differential selectivity

Schmidt's differential sensitivity studies (SADS) [21,31,32] were performed using the 4-iodoanisole/4-iodotoluene and bromoanisole/bromotoluene substrate pairs with the aim to compare the catalytic active species of precatalyst (**4**) with those present when stabilized Pd NPs, or complex (**2**) were used as catalysts. In a typical experiment, the phenyl halide pair (0.25 mmol in each), phenylboronic acid (0.75 mmol), K₂CO₃ (0.75 mmol), the catalyst (≈1% in Pd with respect to the total substrate), and ethanol (50 mL) were introduced into the reactor at 60°. The reaction kinetics was followed by HPLC for the iodoanisole/iodotoluene system according to the general procedure described above. For the 4-bromoanisole/4-bromotoluene pair, the reaction mixture could not be efficiently separated by HPLC. In this case, analyses were carried out by GC (see [supplementary information](#)).

3. Methodology of kinetic data analysis

Concentrations of biphenyl, 4-substituted phenyl halides, and their corresponding 4-substituted biphenylic derivatives were estimated from the chromatographic peak areas using the response factors calculated from the calibration plots. The yield of 4-substituted biphenyl products ($\eta_1(t)$), and biphenyl ($\eta_2(t)$) were calculated by means of Eqs. (1) and (2),

$$\eta_1 = [P_1]/[A]_0 \quad (1)$$

$$\eta_2 = [P_2]/[B]_0 \quad (2)$$

where $[A]_0$ and $[B]_0$ stand for the zero time concentration of 4-substituted phenyl halides and phenylboronic acid, whereas $[P_1]$ and $[P_2]$ represent those of the corresponding 4-substituted biphenyl products and biphenyl respectively. The experimental yields were compared with those calculated from the chemical model shown in Eqs. (3) and (4), which consider the SM cross-coupling and the boronic acid oxidative homocoupling reactions, both of them catalyzed by Pd,



The above formal mechanism has associated the mathematical model consisting of Eq. (5),

$$\frac{d}{dt} \begin{pmatrix} [A] \\ [B] \\ [P_1] \\ [P_2] \end{pmatrix} = \begin{pmatrix} -1 & 0 \\ -1 & -2 \\ 1 & 0 \\ 0 & 1 \end{pmatrix} \times \begin{pmatrix} r_1 \\ r_2 \end{pmatrix} \quad (5)$$

in which r_1 and r_2 are the reaction rates for processes (3) and (4), calculated according to Eqs. (6) and (7),

$$r_1 = k_1(t)[A]^p[B]^q \quad (6)$$

$$r_2 = k_2(t)[B]^2 \quad (7)$$

The value of p and q were set up to 1, according to the results of a previous kinetic study carried out on the Pd NPs-UVM-7 system [25]. In Eqs. (6) and (7), $k_i(t)$ are empirical functions of time taking into account the variation of the catalyst activity along the reaction time interval originated by the change in the concentration of the active Pd species. Specifically, the mathematical expression of such functions is given by Eq. (8),

$$k_i(t) = \frac{a_{i,1} + a_{i,2}t}{1 + a_{i,3}t^2} \quad (8)$$

The concentration profiles predicted by the model were calculated from the numerical integration of the ordinary differential equation system (ODE) depicted by Eq. (5). After substitution of concentration curves into Eqs. (1) and (2), the theoretical yields predicted by the model ($\hat{\eta}_i$) were calculated. Finally, the empirical a_{ij} parameters in Eq. (8) were estimated by minimizing the least-squares predictor ϕ in Eq. (9) with regard these parameters. In Eq. (9), T is the transpose matrix operator.

$$\phi(\mathbf{a}) = \eta\hat{\eta}^T \quad (9)$$

Calculations were performed with an *ad hoc* software developed in our laboratory written in the Julia programming language [33]. Minimization of Eq. (9) was carried out using the Nelder-Mead method [34] implemented in the NLOPT library [35], and integration of the non-stiff ODE in Eq. (5) was performed using the Runge-Kutta like method of Tsitouras [36] implemented in the DifferentialEquations Julia's package [37].

4. Results and discussion

4.1. Precatalyst synthesis and characterization

Scheme 1 summarizes the synthesis procedure. The solvated complex (**3**) was immobilized on the carboxypolystyrene material by reaction with the carboxylate groups that easily replace the acetonitrile molecules. Thus, the palladium complex was covalently tethered to the polymer through bridging carboxylate groups giving the precatalyst $[\text{Pd}_2\{\mu\text{-(C}_6\text{H}_4\text{)PPh}_2\}_2\{\mu\text{-O}_2\text{C(C}_6\text{H}_4\text{-PS)}\}_2]$ labeled as (**4**).

The homogeneous pale yellow color of the precatalyst is a good indication of the complex incorporation on the polymer resin. We have used EDX to assess the presence and stoichiometry of the organometallic Pd complex in the precatalyst as well as the chemical homogeneity of the complex along the polymer matrix, given that a principal objective of our work at this stage was to favor a good dispersion of the precatalytic active sites.

The EDX value were averaged from ca. 50 individual measurements, with a final value corresponding to a Pd/P = 0.98 M ratio. This value fits very well with the expected ratio taking into account that the real anchored species are dimeric complexes with the Pd metal centers connected through two phosphine-related ligands. Our data, also confirm that the precatalyst is chemically homogeneous (at least) at the micro-scale level (spot area of 1 μm^2). Hence, the precatalyst can be considered as monophasic product, and segregation of the organometallic complex can be discarded.

The covalent anchoring through the carboxylate groups of the polymer can be inferred when the IR spectra of the resin and the precatalyst are compared (see [Fig. S1 in supplementary information](#)). In both spectra it can be appreciated several signals in the 700–800, 1000–1100 and around 1500 cm^{-1} that can be assigned to C–H bending out of plane, C–H in plane and C–C stretching vibrations, respectively. The starting resin shows an intense peak (at 1687 cm^{-1}) and an additional signal around 1220 cm^{-1} that can be attributed to C=O and C–OH stretching vibrations of the carboxylate groups. After the complex inclusion, the intensity of

the signals at ca. 1220 cm^{-1} strongly decreases. Moreover, the intense peak at 1687 cm^{-1} disappears and two new signals at 1544 and 1395 cm^{-1} , associated to $\nu_{\text{as}}(\text{O}-\text{C}-\text{O})$ and $\nu_{\text{s}}(\text{O}-\text{C}-\text{O})$ vibrations can be observed. This evolution strongly suggests that the Pd-complexes are effectively anchored on the polymer. The XPS spectrum confirms that the oxidation state of the Pd is preserved after the anchoring step. In fact, the Pd 3d spectrum shows two signals at binding energy values of 337.5 and 342.8 eV (see further below Fig. 7 in Section 4.6) that, according to the bibliography, are due to Pd(II) metal centers.

The STEM-HAADF image in Fig. 1 supports the Pd(II) oxidation state. In fact, only an extremely low number of white spots (due to the presence of Pd(0) nanoparticles) is observed (see below for details). In any case, the mapping on Pd(0)-free domains reveals the presence and homogeneous distribution of Pd and P, now at the nanoscale.

4.2. Catalyst activity

The activity of precatalyst (4) was checked for the SM reaction of boronic acid with the 4-substituted phenylhalides shown in Scheme 2, following the methodology previously described. The Pd(II)-carboxypolystyrene material catalyzed efficiently the reaction at 60 °C. This made a difference with the catalyst Pd NPs-UVM-7 that did not show significant activity below 80 °C [25]. Fig. 2(a) and Fig. S2 (supplementary information) show the kinetic behavior of 4-substituted phenyl bromides and phenyl iodides respectively. The reactivity order was that expected for a SM reaction controlled by the transmetalation step (i.e. the reaction became faster when increasing the substituent electronegativity for substrates sharing the same halide) [38–40]. As expected, the rate for 4-substituted phenyl iodides was higher than that of their corresponding bromo derivatives due to the left-displacement that occurs in the oxidative addition equilibrium involving the phenyl bromides. The equilibrium shift was caused by the higher energy of the C–Br bond in relation to that of the C–I bond.

Fig. 2(b) shows the variation in activity of the catalyst quantified by means of the $k(t)$ function, which reflects the change in the nature and concentration of the Pd species inside the reactor [41,42]. The basic idea behind this methodology is the assumption that all Pd species (in the liquid phase and anchored on the catalyst surface) have different activities (k_i), so that the observed catalytic activity is calculated as the sum of that of all species,

$$-\frac{d[A]}{dt} = \left(\sum_i k_i x_i(t) \right) [\text{Pd}]_T [A][B] = k(t) [\text{Pd}]_T [A][B] \quad (10)$$

The first-order dependence of Eq. (10) on the analytical concentration of Pd ($[\text{Pd}]_T$) was checked (see Fig. S3 in supplementary information). Obviously, if the mole fraction of Pd species ($x_i(t)$) varies, e.g. due to dissolution, aggregation, or deposition processes, the activity of the catalyst will change over time [43]. The function inside the summatory requires a detailed knowledge of the distribution of Pd species and their specific activity. Usually, the last information is not experimentally available and, for this reason, the empirical $k(t)$ function was used in this work to perform a semi-quantitative analysis of the activity. Table 1 collects the calculated parameters defining the catalyst activity namely, the value of $k(t)$ (k_{max}), the formal catalytic constant ($k_{\text{cat}} = k_{\text{max}}/[\text{Pd}]_T$), the turnover frequency at the maximum activity ($\text{TOF} = k_{\text{max}}[A][B]/[\text{Pd}]_T$), and the experimental yields of the SM products and biphenyl at 5 h.

Remarkable differences in activity were found for the silica and polymer supported catalysts. All reactions catalyzed by the polymeric material exhibited an induction period, their activity $k(t)$ curves going through a maximum as shown in Fig. 2(b). This extreme was absent for the silica-supported material, for which

$k(t)$ were found to be monotonically decreasing functions with maximum rate at zero time [25]. In general, the silica supported catalyst presented higher activities for 4-substituted phenyl iodides. However, this type of catalysts undergone rapid deactivation, leading to particularly low yields when using phenyl bromide derivatives substituted with electrodonor radicals as substrates ($\eta_1(24\text{h}, 80\text{ °C}) = 34, 16, 10\%$ for Br-Ph-R with R = H, OCH_3 , CH_3 [25]). This issue makes the material of little interest to catalyze reactions involving low activated phenyl halides. Although the polymeric material reacted more slowly for 4-substituted phenyl iodides, it was quite more active for 4-substituted phenyl bromides than the silica-supported material. Even more interesting was the fact that the yields for the polymer supported system were higher for all substrates (e.g. $\eta_1(5\text{h}, 60\text{ °C}) = 87, 76, 68\%$ for Br-Ph-R with R = H, OCH_3 , CH_3), which makes the use of the polymeric support especially attractive when using weakly activated phenyl halides.

The induction period suggested that Pd(II) is not the active catalyst, and hence Pd(II) complexes in material (4) must undergo reduction. The activity was rationalized assuming that small amounts of Pd atoms coming from the Pd(II) reduction enter into the solution, starting the SM catalytic cycle. The activity increases while the reduction in progress supplies Pd atoms. On the other hand, the aggregation process leads to a gradual activity loss as the solubilized Pd species form larger aggregates. Obviously, the activity curves must go through a maximum as a consequence of the opposite effect caused by the reduction/aggregation processes. This behavior differs from that observed for the Pd NPs-UVM-7 catalyst. For this material, Pd(0) enters massively the dissolution as small Pd NPs when the reactor reaches a critical temperature (80 °C), resulting in a high initial reaction rate. Nevertheless, the activity drops rapidly due to the aggregation phenomenon, which occurs in a greater extent because of the higher Pd(0) concentration in the solution.

The difference in activity for phenylbromides presented by the polymeric material and Pd NPs-UVM-7 can be understood by analyzing the way in which the material introduces the Pd active species in the medium. The polymer-immobilized catalyst provides small amounts of Pd atoms continuously, hence it catalyzes the reaction as long as the polymer is capable to do this task. In contrast, the silica material delivers most of Pd(0) as Pd NPs at the beginning of the reaction. As mentioned, the Pd NPs aggregate faster as they are larger and more concentrated, resulting in an earlier depletion of the most active Pd species. These differences are also related to the different nature of the materials: porous vs. non-porous when the silica or the polymer is used as support. In order to provide Pd NPs, the polymer needs first to be swollen through the solvent action, then forming the Pd(0) species, and finally diffuse (more hindered when compared to the open bimodal pore system of the UVM-7). The other determinant factor is the relative rate of the aggregation respect to the reaction rate. If the aggregation process is faster than the chemical reaction, the early depletion of the active Pd will cause a decrease in the reaction yield. In this line, the yield of the slow reacting bromo derivatives is higher when using the catalyst immobilized on the polymer, as the active species are not exhausted throughout the course of the reaction, whereas the decrease in yield was not observed for the faster reacting 4-iodo phenyl derivatives, all of them reaching near 100% conversion.

4.3. Reusing catalyst experiments

Fig. 3(a) and (b) shows the change of yield and activity along 6 reusing cycles. All the graphs indicated that the activity remained high and constant during the first 4 cycles, observing an abrupt decrease from the fifth one, and the activity declining until a prac-

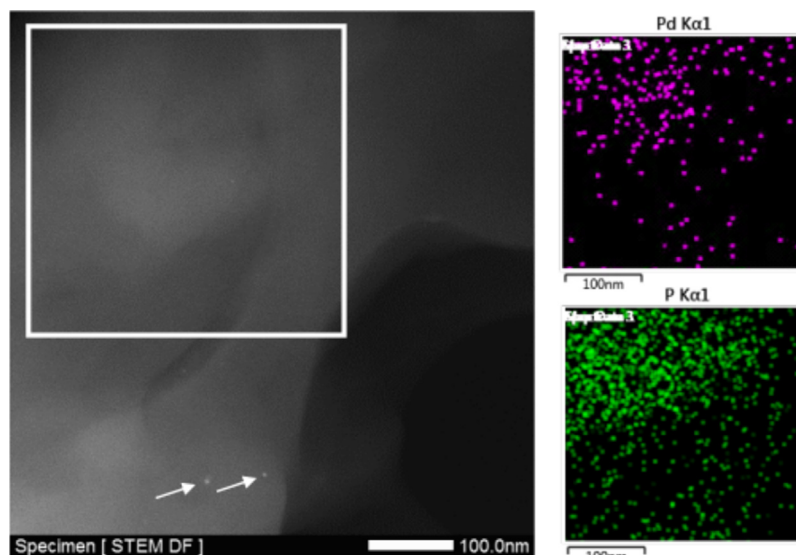
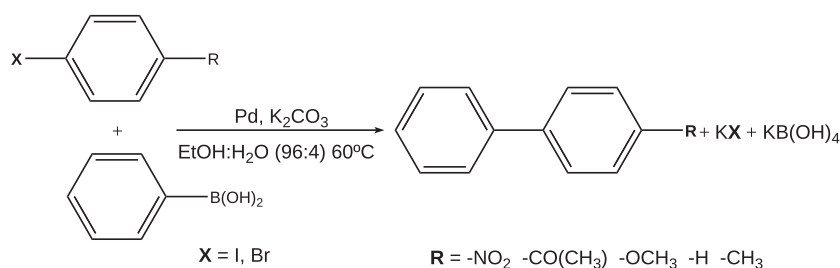


Fig. 1. STEM-HAADF image of the pre-catalyst containing the Pd binuclear organometallic complex anchored on the polymer surface. Arrows mark white spots associated with isolated and sparse Pd NPs. The mapping carried out on the white square shows the presence of Pd and P dispersed along the polymer.



Scheme 2. The Suzuki-Miyaura reaction.

tically null value by the 6th cycle. The observation was consistent with the palladium-reservoir role played by the material. Correlating with the activity loss, the appearance of the recovered material varied from the bright yellow of the catalyst before use (originated by the phosphine Pd(II) complexes) to the dark gray of the material recovered after the 6th cycle. This change in color clearly indicated a progressive reduction of the Pd(II) complexes, and the subsequent deposition of Pd(0) on the polymer during the cooling/centrifugation processes carried out between cycles. The effect of using a polycarboxystyrene polymer with double load of catalyst is shown in Fig. S4 (see supplementary information). Higher activity was observed together with a slower deactivation of the material along the cycles.

Table 2 collects the relative abundance of P, Pd, and K determined from scan electron microscopy (SEM) for the first, third, and sixth reusing cycles (see Figs. S5 and S6 in supplementary information). The P signal was originated by the phosphine complexes, whereas the Pd signal was originated by both the Pd(II) bound to phosphorus (ratio P/Pd is 1:1) and the Pd(0) deposited on the polymer. Consequently, the ratio P/Pd was proportional to the mole fraction of Pd(II). SEM analysis indicated that Pd was found mainly as Pd(II) (96%) after the first cycle, this amount decreasing to 73% after the third one. Composition drastically changed after the sixth cycle, where the P signal was practically absent, therefore the catalyst consisting of Pd(0) mostly. These results also suggested that Pd(II) reduction implied the removal of the phosphine ligands from polystyrene. The results are indicative that the SM reaction is occurring as long as the catalyst con-

tains a certain pool of Pd(II). Additionally, Pd(0) aggregates formed along cycles have little or null activity as evidenced by the lack of activity of 6th cycle, for which Pd(II) is exhausted but the material is still containing Pd(0). Therefore, kinetic results and SEM analysis allow concluding that the Pd(0) formed/solubilized along the reaction probably supports most of the catalytic action.

4.4. Classical tests to check the homogeneous vs. heterogeneous nature of the catalysis

The question raised now is how Pd(0) develops its catalytic action. One possibility is that the Pd(0) fixed on the polymer surface is the active catalyst, or, at the other end, the catalysis is basically driven by the solubilized fraction of Pd(0). With the aim to investigate this issue, the classical hot-filtrate and centrifugation tests were carried out according to the procedures described previously.

Hot filtration and centrifugation experiments. Fig. S7 (see supplementary information) shows the evolution of the reaction mixture before and after the filtration process when using 4-methoxyiodobenzene as the substrate. The reaction stops completely in the filtrate, while it continues in the flask whose reactants are in contact with the catalyst. Analogous comments can be made after the observation of Fig. S8 (see supplementary information), where the results related to the centrifugation test are shown.

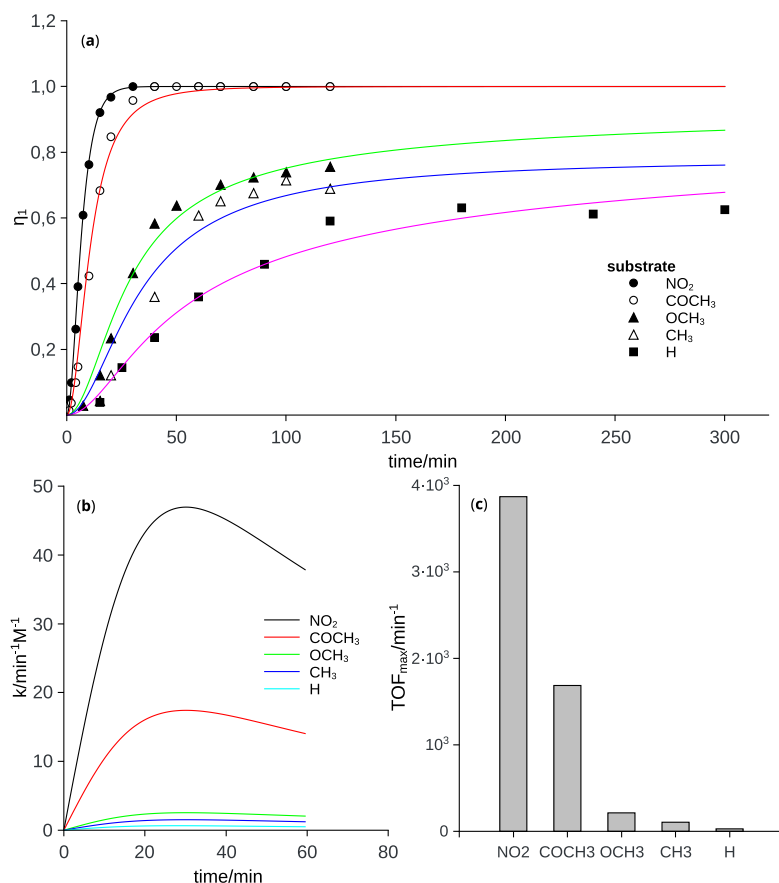


Fig. 2. (a) Change with time of the reaction yield for the tested 4-substituted phenyl bromides indicated at the plot legend catalyzed by precatalyst (4). Solid lines were calculated by fitting the experimental yields (symbols) to the mathematical model defined by Eqs. (3)–(5); (b) estimated variation of $k_i(t)$ calculated from Eq. (8); (c) turn-over frequency estimated at the maximum catalyst activity.

Table 1

Kinetic and statistical fitting parameters for the SM reaction for the studied 4-substituted phenylhalides ($\text{X}-\text{C}_6\text{H}_4-\text{R}$) catalyzed by precatalyst (4).^a

X	R	$k_{\text{max}}/\text{min}^{-1}\text{M}^{-1}$	$k_{\text{cat}} \times 10^{-4}/\text{min}^{-1}\text{M}^{-2}$	$\text{TOF}_{\text{max}} \times 10^{-3}/\text{h}^{-1}$	$\eta_1(5\text{ h})^{\text{b}}$	$\eta_2(5\text{ h})^{\text{b}}$	R	LOF(%) ^c
I	COCH_3	23	23	2.4	100	0	0.9991	3.3
	OCH_3^{d}	8.5	8.0	0.7	99	4.7	0.9994	2.9
	CH_3	6.4	6.4	0.5	99	0	0.997	6.5
	H	11	11	1.0	99	0	0.9998	1.8
Br	NO_2	47	44	3.9	100	11	0.9999	1.3
	COCH_3	17	16	1.7	100	0	0.9993	3.3
	OCH_3	2.5	2.4	0.2	87	6.3	0.990	11
	CH_3	1.6	1.4	0.1	76	24	0.990	12
	H	0.6	0.6	0.03	68	0	0.995	7.6

^a In all kinetic runs: $[\text{Pd}] = 1.0 \times 10^{-4} \text{ mol/L}$.

^b η_1 : SM reaction yield, η_2 : biphenyl yield.

^c LOF: lack of fit in %.

^d A turn-over number of 125 mol substrate/mol catalyst was calculated for the 4-iodoanisole substrate (see [supplementary information](#)).

We may be tempted to conclude that the reaction is mainly driven by the $\text{Pd}(0)$ clusters existing on the surface of the catalyst. However, if that is the case, it is difficult to understand why the material isolated in cycle 6 does not exhibit any catalytic activity. An alternative explanation is to admit that the solubilized species of $\text{Pd}(0)$ suffer a coalescence process in solution during filtering upon lowering the temperature that causes their deposition on the polymeric material (“boomerang system”) [16]. According to previous assumptions the catalysis would be mainly conducted by the solubilized $\text{Pd}(0)$ and, consequently, the lack of activity of the filtrate would be a consequence of the Pd removal during the cooling/filtering/centrifugation processes. It is obvious that results

of filtration and centrifugation tests were not conclusive due to the possibility of Pd elimination from solution during the sample handling. In order to demonstrate the existence of active Pd within the solution, two additional tests were carried out, namely the Pd -poisoning and the three phase tests.

Poisoning catalyst test. Fig. S9 (see [supplementary information](#)) shows that the reaction stops just after the Quadrapure TU (poison) addition (50 min) [31,44]. By this time, the product yield stabilizes at 64% that differs from the 85% value observed at 50 min for the reaction carried out in absence of poison. Concurring with the hypothesis raised above, this result strongly suggests that the solubilized Pd fraction is the main responsible for the catalytic action.

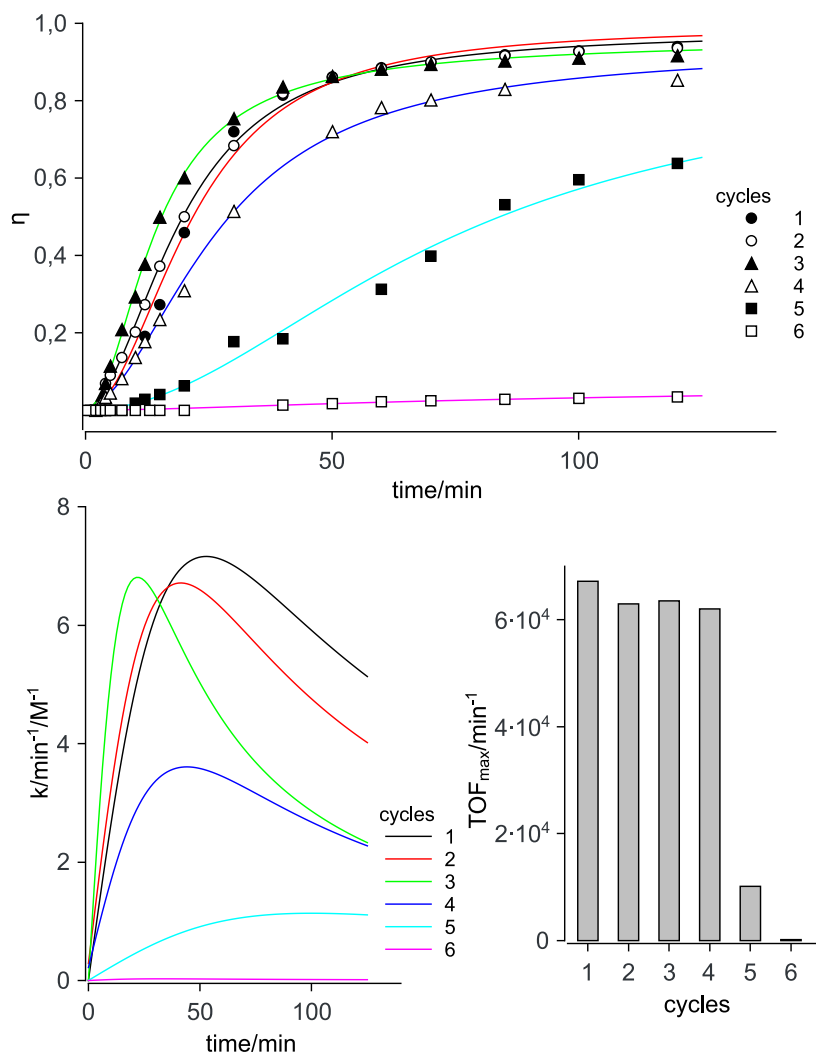


Fig. 3. (a) Time variation of the SM reaction yield for the 4-methoxyphenyl iodide along the several reusing cycles displayed at the plot legend catalyzed by precatlyst (**4**). Solid lines were calculated by fitting the experimental yields (symbols) to the mathematical model defined by Eqs. (3)–(5); (b) estimated variation of $k_1(t)$ calculated from Eq. (8); (c) turn-over frequency estimated at the maximum catalyst activity.

Table 2

Relative abundance of P, Pd, and K atoms (in %) in precatlyst (**4**) calculated from SEM analysis for selected reusing cycles.

Cycle	P	Pd	K ^b	P/Pd
1 ^a	4.9	5.1	90	0.96
3	22.4	30.5	47.1	0.73
6	0.04	14.9	85.1	0.002

^a Catalyst before use.

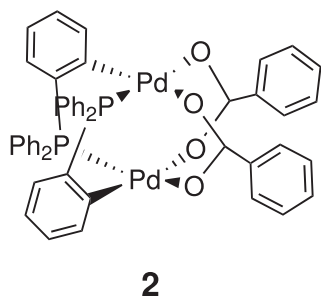
^b The K signal resulted unhelpful for the catalyst characterization as there were two potassium sources, namely the carboxylate groups of the resin ($\text{COO}^- \text{K}^+$), and a variable amount of K_2CO_3 residues that remained on the surface after the washing process.

Three phases test. Fig. S10(b) (supplementary information) shows ^1H NMR spectrum of the reaction mixture after the hydrolysis treatment, which was fully consistent with the presence of 4-bromobenzoic acid (signals at 7.98 and 7.64 ppm, integration ratio 2:2) and [1,1'-biphenyl]-4-carboxylic acid (signals at 8.19, 7.72, and 7.51 ppm, integration ratio 2:2:3) in an approximate ratio 70:30. The detection of [1,1'-biphenyl]-4-carboxylic acid confirmed that the solubilized Pd species are involved in the catalytic process.

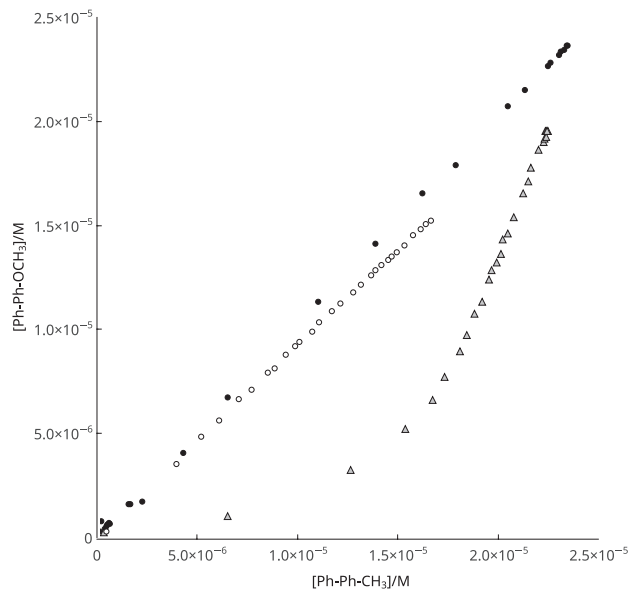
4.5. Schmidt's analysis of differential selectivity

The SADS test allows comparing the active species of two catalysts. If one of them is immobilized and the other is in solution, the test will allow differentiating when the catalytic action is carried out by the solubilized fraction of Pd or by that immobilized on the polymeric support. The test consists of two kinetic runs carried out in identical experimental conditions but differing in the catalyst used. For this purpose, the behavior of precatlyst (**4**) was compared with the molecular compound (**2**) (see Scheme 3), and with the stabilized Pd NPs. These Pd NPs showed sizes lower than 5 nm and were stabilized by the PVP polymer (see Fig. S13 in supplementary information). In each experiment, two phenyl halides were simultaneously reacted until their complete depletion, and the concentration of the corresponding biaryl products (P_1 and P_2) was measured along the reaction time. The concentration of P_1 was plotted against that of P_2 so that the coincidence of the trajectories on the phase plane ($[\text{P}_1], [\text{P}_1]$) ensured that both catalysts shared the same active species. On the contrary, if the catalysts were driven by dissimilar Pd species, then a notable divergence between trajectories should be observed.

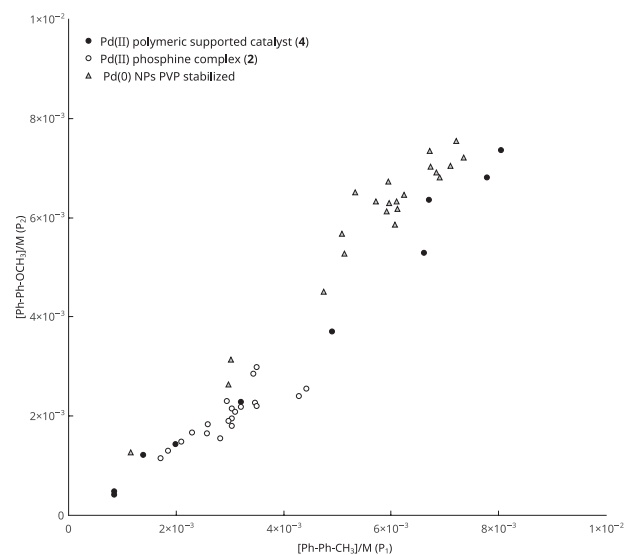
Fig. 4(a) shows that the trajectories associated with the immobilized material and stabilized Pd NPs consist of straight lines of



Scheme 3. Structure dinuclear Pd(II) complex.



(a) 4-iodoanisole and 4-iodotoluene



(b) 4-bromoanisole and 4-bromotoluene

Fig. 4. SADS plots for the SM reaction of (a) 4-iodoanisole/4-iodotoluene and (b) 4-bromoanisole/4-bromotoluene with phenylboronic acid at 60° in ethanol catalyzed by materials (4), (2), and Pd NPs stabilized with PVP.

similar slope for a SADS experiment performed with 4-iodoanisole and 4-iodoacetophenone as substrates. They differ significantly from the curved trajectory shown by complex (2), see Scheme 3.

The conclusion to be drawn is that the catalytic active species of the Pd(II) supported polymer and stabilized Pd NPs must be very similar, i.e. the catalysis must be driven by the solubilized Pd(0), and hence the Pd(II) supported on the polymer is acting as a mere Pd(0) supplier. Furthermore, the SADS diagram allows discarding the supply of active Pd(II) phosphine complexes to solution from the resin, as in such a case the trajectory associated with the immobilized catalyst should be superimposed on that of (2). A SADS experiment using 4-bromotoluene and 4-bromoanisole as substrates yielded similar results, see Fig. 4(b). For this system, however, the three catalysts exhibited linear SADS plots suggesting that both Pd(II) complexes (2 and 4) reduce to Pd(0). This behavior can be rationalized assuming that the lower reaction rate of bromoderivatives allows for the previous reduction of (2) in the homogeneous phase.

Fig. S11 (supplementary information) shows the yield in the biaryl product of the 4-iodoanisole measured from the SADS experiment when using as catalysts the immobilized material (4), and stabilized Pd NPs. It is apparent that the difference between both materials lies in the induction period (present only in the immobilized catalyst), the conversion, which reaches practically 100 % in the case of the immobilized complex, but reaching only 60 % for the stabilized Pd NPs, and the initial reaction rate, which is clearly greater for the Pd(0) NPs material. Again, the differences in activity can be rationalized if it is assumed that the solubilized fraction of Pd(0) is the one with the highest catalytic activity. Indeed, Pd NPs exhibit initially a high reaction rate as they consist basically of stabilized Pd(0) nanoclusters. On the contrary, an induction period is observed for the immobilized material caused by the time it takes to reduce some of Pd (II), which slows down the conversion rate due to the lack of active Pd during the initial phase of the reaction. Finally, the observed difference in the biaryl product yields should arise from the different rates of other processes not related directly to the main catalytic cycle [45]. Probably, PVP induces Pd(0) aggregation better than the carboxylic resin, whereby the stabilized suspension of Pd NPs deactivates faster than material (4).

4.6. STEM-HAADF characterization of the catalyst along the reusing cycles

The evolution of the catalyst after consecutive cycles has been also analyzed by electron microscopy and XPS. Hence, STEM-HAADF images of the catalyst between the first and the fifth cycle have been gathered in Fig. 5. No significant differences appear during the first four cycles. The polymer surface seems to be decorated with small white spots associated to the formation of PdNPs. Together with small pseudospherical particles with sizes in the 5–7 nm range, larger additional elongated, irregular and curved spots also appears from the first catalytic cycle. The irregular and variable shape of these spots is suggestive of nanoparticle aggregation more than particle growing. In any case, we observe a certain tendency related to the size of the larger aggregates detected as the catalytic cycles increases: these clusters evolve from 25–35, to 50–65 and up to more than 100 nm for the catalyst after cycles 1 and 2, 3 and 4, and finally after 5 cycles, respectively. In a parallel way, the density of small Pd NPs slightly decreases after the fourth cycle and more abruptly after the fifth cycle. In order to illustrate this point, the Pd NPs size distribution for each cycle is shown in Fig. S14 (supplementary information). In addition to the Pd(0) NPs detected through STEM-HAADF, a certain proportion of Pd (probably as anchored complexes) remains trapped inside the polymer. Its presence is evident in the mapping done in domains where white spots do not appear. The polymer is not porous and shows a low surface area of ca. 2 m²/g. Then, cannot be discarded that a low ratio of Pd organometallic complexes could be anchored

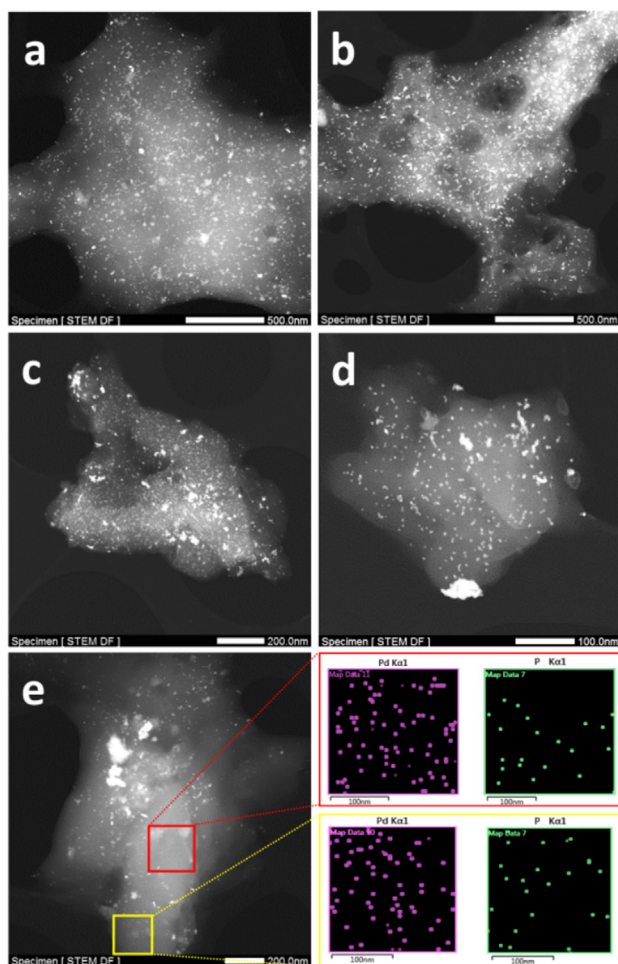


Fig. 5. STEM-HAADF images of the catalyst after (a) one, (b) two, (c) three, (d) four and (e) five catalytic cycles. The white spots correspond to Pd nanoparticles or aggregates thereof. The persistence of Pd and P in free-Pd NPs areas (without white spots) is shown in the mapping performed to the catalyst after 5 reaction cycles.

but also trapped inside the polystyrene resin without any possibility to be chemically reduced and consequently unable to form or participate in the nucleation and growth of metal nanoparticles. In this sense, the polymer must be viewed as a reservoir of Pd complexes that during the first four or five catalytic cycles evolves through the formation of active Pd NPs up to exhaust of the accessible complexes or the aggregation of the nanoparticles. The formation of particle aggregates can be clearly appreciated in the HRTEM images shown in Fig. 6. These micrographs are consistent with the STEM-HAADF data. The observation of aggregates occurs even during the first cycles leading to relatively small clusters with different and irregular distributions in which the real “building blocks” are pseudospherical nanoparticles with very small averaged sizes comprises in the 3–4 nm range. As the number of catalytic cycles increases, a significant growth of this aggregates occurs, but preserving the size of the primary Pd NPs. This small crystallite size is consistent with the absence of XRD signals regardless the number of cycles (and the aggregation degree).

The evolution of the Pd 3d XPS spectra (Fig. 7) is consistent with the electron microscopy data and also with the kinetic study. After the first catalytic cycle, the dominant signals in the XPS spectrum fits very well with the peaks detected for the pre-catalyst. Then, in the recovered solid after cycle 1, Pd(II) is the dominant oxidation state, which must correspond to the existence of Pd organometallic complexes anchored to the resin. This does not exclude that a

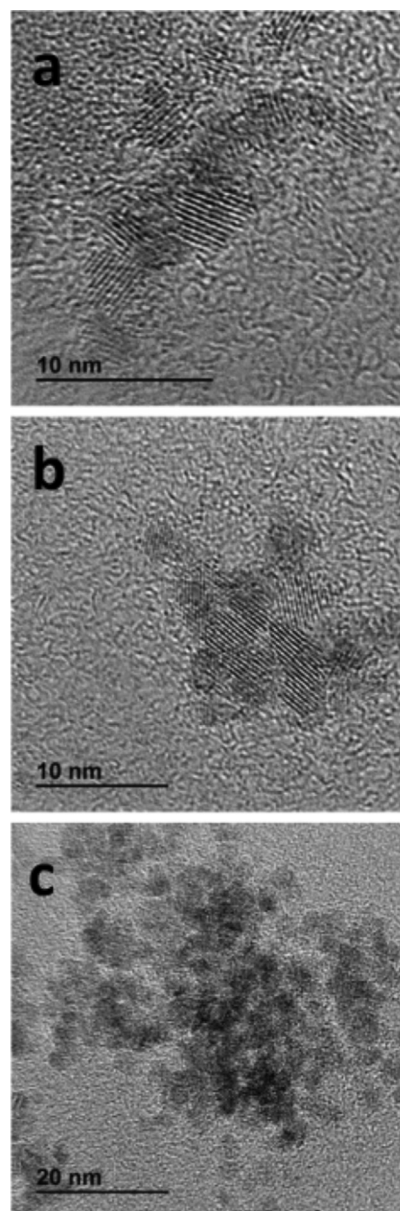


Fig. 6. HRTEM images of the catalyst after (a) one, (b) three and (c) four catalytic cycles.

certain proportion of Pd was reduced forming Pd NPs. A part of these Pd NPs could be eliminated during the filtration step, and the rest remains on the resin support (according to the STEM-HAADF images). In any case, what is obvious is that a large proportion of Pd organometallic complexes remain anchored to the resin as seminal catalytic building blocks. From the second cycle, the Pd 3d XPS signals attributed to Pd(0) can be clearly observed and its relative intensity increases in a regular way with the catalytic cycles. This evolution can almost be better understood as a progressive reduction of the Pd(II) complexes trapped within the resin. The catalysts act as a reservoir of palladium that due to the non-porous nature of the resin (in contrast with the Pd NPs-UVM-7 silica case) shows a certain inertia towards the attack to the complex what it means to lose the anchorage, the reduction of palladium and its subsequent nucleation and growth forming Pd NPs (or aggregates). The Pd NPs in solution and/or decorating the resin surface must be the effective catalytic sites. Until the fourth cycle, the STEM-HAADF images are quite similar: a good dispersion of Pd

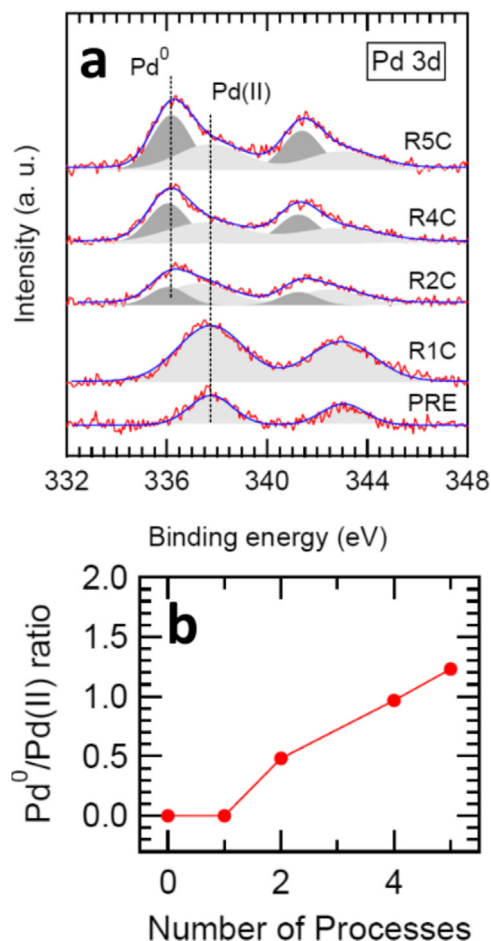


Fig. 7. (a) Evolution of the Pd 3d XPS spectra with the number of progressive catalytic cycles (PRE = precatalyst; RnC, n = 1, 2, 3, 4 and 5, n = number of catalytic cycles). (b) Evolution of the Pd⁰/Pd(II) ratio with the number of catalytic cycles.

NPs or small aggregates is observed (although it is true that the size of the latter and their abundance increase progressively with the number of cycles). After the fifth cycle, Pd(0) is the dominant species. However, the catalytic activity drops abruptly. It is also after the fifth cycle when more important differences are seen in STEM-HAADF images. As previously commented, the density of Pd NPs on the surface resin decreases and large aggregates are observed (these latter are probably not able to act as effective catalytic centers). This evolution can be understood as an exhaustion of the accessible Pd reserve. A certain amount of Pd complexes will resist trapped within the resin according to XPS and the mapping images.

5. Conclusions

The new material [Pd₂{μ-(C₆H₄) PPh₂}₂{μ-O₂C(C₆H₄-PS)}₂] (**4**) containing the organometallic complex (**2**) covalently linked to a carboxypolystyrene support was prepared through a synthetic route that allows the Pd(II) cations to be dispersed homogeneously on the polymer surface.

The activity was checked for the Suzuki-Miyaura reaction. The conversion-time plots exhibited an induction period originated by the reduction of Pd (II) to Pd (0), and their analysis indicated that the activity went through a maximum along the reaction time. This phenomenon was explained by the continuous delivery of Pd atoms to the solution from the polymeric support and the subsequent deactivation by aggregation of the solubilized fraction of

Pd. The catalysis was driven mostly by Pd(0) species in solution, as assessed by the three phases test and the differential sensitivity kinetic assay results. The activity of material (**4**) compared to that of Pd NPs-UVM-7 resulted in slightly lower conversion rates for 4-phenyliodides, but higher conversions for 4-phenylbromides even operating at lower temperatures. Comparison with PVP stabilized Pd NPs revealed a similar behavior as material (**4**) presented lower initial rates but enhanced conversion yields. Hence, the ability of the material (**4**) to supply continuously Pd(0) to the medium made it a more suitable catalyst, specially when using weakly activated phenyl halides as substrates.

The catalyst reusing experiments showed that activity of material (**4**) remained at the same level for the first 4 cycles making a difference with Pd NPs-UVM-7 [25] and PVP stabilized Pd NPs (Pd NPs were remarkably deactivated during the first cycle, see Figure S11), which lost notably their catalytic activity along the first cycle. Palladium deposited on the support during the cooling/filtering of the reaction mixture, resulting in filtrates without catalytic activity. The structural study of the recovered catalyst was consistent with the kinetic study. Thereby, SEM and XPS studies showed a progressive reduction in the Pd(II)/Pd(0) ratio, and STEM-HAADF showed that Pd NPs size increased through the cycles, both phenomena being correlated with an activity fall. The structural analysis suggested that the larger less active Pd NPs were not formed by crystal growth, but rather by aggregation of smaller Pd NPs, probably in solution.

Acknowledgments

We thank the Spanish Ministerio de Economía y Competitividad and European Feder Funds (MAT2015-64139-C4-2-R and RTI2018-100910-B-C44) for funding this research.

Appendix A. Supplementary material

Figure S1: FTIR spectra of (**4**); Figure S2: Catalytic activity of phenyliodides; Figure S3: Influence of catalyst concentration in reaction rate; Figure S4: Results of a reusing experiment using a double load Pd catalyst; Figures S5/S6: SEM results; Figure S7: hot filtration classical test results; Figure S8: Centrifugation classical test results; Figure S9: Poisoning test results; Figure S10: Three phases test results; Figure S11: SADS kinetics for phenyliodide derivatives. Figure S12: Deactivation of the catalyst by continuous addition of substrate; Figure S13: TEM micrographs of PVP stabilized Pd NPs; Figure S14: NPd NPs distribution size for the diverse reusing catalyst cycles. Supplementary data associated with this article can be found, in the online version, at <https://doi.org/10.1016/j.jcat.2019.10.014>.

References

- [1] N. Miyaura, A. Suzuki, Palladium-catalyzed cross-coupling reactions of organoboron compounds, *Chem. Rev.* 95 (1995) 2457–2483.
- [2] D.S. Surry, S.L. Buchwald, Dialkylbiaryl phosphines in Pd-catalyzed amidation: a user's guide, *Chem. Sci.* 2 (2011) 27–50.
- [3] R. Chinchilla, C. Nájera, Recent advances in Sonogashira reactions, *Chem. Soc. Rev.* 40 (2011) 5084–5121.
- [4] J. Corbet, G. Mignani, Selected patented cross-coupling reaction technologies, *Chem. Rev.* 106 (2006) 2651–2710.
- [5] J. Magano, J. Dunetz, Large-scale applications on transitions metal-catalyzed coupling for synthesis of pharmaceuticals, *Chem. Rev.* 111 (2011) 2177–2250.
- [6] C. Torbog, M. Beller, Recent applications of palladium-catalyzed coupling reactions in the pharmaceutical, agrochemical, and fine chemistry industries, *Adv. Synth. Catal.* 352 (2009) 3027–3043.
- [7] R. Chinchilla, C. Nájera, Chemicals from alkynes with palladium catalysts, *Chem. Rev.* 114 (2014) 1783–1826.
- [8] L. Yin, J. Liebscher, Carbon-carbon coupling reactions catalyzed by heterogeneous palladium catalysts, *Chem. Rev.* 107 (2007) 133–173.

- [9] V. Polshettiwar, C. Len, A. Fihri, Silica-supported palladium: Sustainable catalysts for cross-coupling reactions, *Coord. Chem. Rev.* 253 (2009) 2599–2626.
- [10] M. Lamblin, L. Nassar-Hardy, J. Hierso, E. Fouquet, F. Felpin, Recyclable heterogeneous palladium catalysts in pure water: Sustainable developments in Suzuki, Heck, Sonogashira and Tsuji-Trost reactions, *Adv. Synth. Catal.* 352 (2010) 33–79.
- [11] N.E. Leadbeater, M. Marco, Preparation of polymer-supported ligands and metal complexes for use in catalysis, *Chem. Rev.* 102 (2002) 3217–3274.
- [12] B. Altava, M.I. Burguete, E. Garcí-Verdugo, S.V. Luis, Chiral catalysis immobilized on achiral polymers: effect of the polymer support on the performance of the catalyst, *Chem. Soc. Rev.* 47 (2018) 2722–2771.
- [13] E. Mohammadi, B. Movassagh, Synthesis of polystyrene-supported Pd(II)-NHC complex derived from theophylline as an efficient and reusable heterogeneous catalyst for the Heck-Masuda cross-coupling reaction, *J. Mol. Catal. A: Chem.* 418 (2016) 158–167.
- [14] M. Bakherad, B. Bahramian, S. Jajarmi, A novel 1,2,4-triazine-functionalized polystyrene resin-supported Pd(II) complex: a copper- and solvent-free highly efficient catalyst for Sonogashira coupling reactions, *J. Organomet. Chem.* 749 (2014) 405–409.
- [15] V.N. Mikhaylov, V.N. Sorokoumov, K.A. Korvinson, A.S. Novikov, I.A. Balova, Synthesis and simple immobilization of palladium(II) acyclic diaminocarbene complexes on polystyrene support as efficient catalysts for Sonogashira and Suzuki-Miyaura cross-coupling, *Organometallics* 35 (2016) 1684–1697.
- [16] V.N. Mikhaylov, V.N. Sorokoumov, D.M. Liakov, A.G. Tskhovrebov, I.A. Balova, Polystyrene-supported acyclic diaminocarbene palladium complexes in Sonogashira cross-coupling: Stability vs. catalytic activity, *Catalysts* 8 (2018) 141–159.
- [17] M.V. Polynski, V.A. Ananikov, Modeling key pathways proposed for the formation and evolution of “cocktail”-type systems in Pd-catalyzed reactions involving ARX reagents, *ACS Catal.* 9 (2019) 3991–4005.
- [18] S. Hüber, J.G. de Vries, V. Farina, Why does industry not use immobilized transition metal complexes as catalysts?, *Adv Synth. Catal.* 358 (2016) 3–25.
- [19] L. Falivene, S.M. Kozlov, L. Cavallo, Constructing bridges between computational tools in heterogeneous and homogeneous catalysis, *ACS Catal.* 8 (2018) 5637–5656.
- [20] L. Liu, A. Corma, Metal catalysts for heterogeneous catalysis: from single atoms to nanoclusters and nanoparticles, *Chem. Rev.* 118 (2018) 4981–5079.
- [21] A. Biffis, P. Centomo, A. Del Zotto, M. Zecca, Pd metal catalysts for cross-couplings and related reactions in the 21st century: a critical review, *Chem. Rev.* 118 (2018) 2249–2295.
- [22] A.A. Kurokhtina, E.V. Larina, A.F. Shmidt, Study of the differential selectivity of cross-coupling reactions for elucidating the nature of the true catalyst, *Kinet. Catal.* 56 (2015) 191–197.
- [23] D.B. Eremin, V.P. Ananikov, Understanding active species in catalytic transformations: from molecular catalysis to nanoparticles, leaching, “cocktails” of catalysts and dynamic systems, *Coord. Chem. Rev.* 346 (2017) 2–19.
- [24] J. El Haskouri, J.M. Morales, D. de Zárate, L. Fernández, J. Latorre, C. Guillem, A. Beltrán, D. Beltrán, P. Amorós, Nanoparticulated silicas with bimodal porosity: chemical control of the pore sizes, *Inorg. Chem.* 47 (2008) 8267–8277.
- [25] P. Alfonso Albiñana, J. El Haskouri, M.D. Marcos, F. Estevan, P. Amorós, M. Úbeda, F. Pérez-Pla, A new efficient, highly dispersed, Pd nanoparticulate silica supported catalyst synthesized from an organometallic precursor. Study of the homogeneous vs. heterogeneous activity in the Suzuki-Miyaura reaction, *J. Catal.* 367 (2018) 283–295.
- [26] F. Estevan, A. García-Bernabé, P. Lahuerta, M. Sanaú, M.A. Úbeda, M.C. de Arellano, Synthesis, reactivity, and X-ray crystallographic characterization of mono-, di-, and tetranuclear palladium(II)-metalated species, *Inorg. Chem.* 39 (2000) 5964–5969.
- [27] F. Estevan, S. Ibañez, P. Hirva, A. Ofori, M. Sanau, M. Úbeda, Benzoate and thiobenzoate ligands in the synthesis of palladium(III) and (II) compounds: stability and catalytic applications, *Eur. J. Inorg. Chem.* (2015) 2822–2832.
- [28] C.M. Crudden, M. Sateesh, R. Lewis, Mercaptopropyl-modified mesoporous silica: a remarkable support for the preparation of a reusable, heterogeneous palladium catalyst for coupling reactions, *J. Am. Chem. Soc.* 127 (2005) 10045–10050.
- [29] M.L. Kantam, M. Roy, S. Roy, B. Sreedhar, S.S. Madhavendra, B.M. Choudary, R.L. De, Polyaniline supported palladium catalyzed Suzuki-Miyaura cross-coupling of bromo- and chloroarenes in water, *Tetrahedron* 63 (2007) 8002–8009.
- [30] H. Gruber-Woelfler, P.F. Radaschitz, P.W. Feenstra, W. Haas, J.G. Khinast, Synthesis, catalytic activity, and leaching studies of a heterogeneous Pd-catalyst including an immobilized bis(oxazoline) ligand, *J. Catal.* 286 (2012) 30–40.
- [31] A.F. Schmidt, A.A. Kurokhtina, Distinguishing between the homogeneous and heterogeneous mechanisms of catalysis in the Mizoroki-Heck and Suzuki-Miyaura reactions: Problems and prospects, *Kinet. Catal.* 53 (2012) 714–730.
- [32] A.F. Schmidt, A.A. Kurokhtina, E.V. Larina, Simple kinetic method for distinguishing between homogeneous and heterogeneous mechanisms of catalysis, illustrated by the example of “ligand-free” Suzuki and Heck reactions of aryl iodides and aryl bromides, *Kinet. Catal.* 53 (2012) 86–93.
- [33] J. Bezanson, S. Karpinski, V.B. Shah, A. Edelman, Julia: A fast dynamic language for technical computing, *CoRR* abs/1209.5 (2012).
- [34] J.A. Nelder, R. Mead, A Simplex method for function minimization, *Comput. J.* 7 (1965) 308–313.
- [35] S.G. Johnson, The NLOPT nonlinear-optimization package, 2012, <http://ab-initio.mit.edu/nlopt>. <http://ab-initio.mit.edu/nlopt>.
- [36] C. Tsitouras, T. Simos, Explicit high order methods for the numerical integration of periodic initial-value problems, *Appl. Math. Comput.* 95 (1998) 15–26.
- [37] Y. Nishihara, Q. Nie, *Differentialequations.jl - a performant and feature-rich ecosystem for solving differential equations in Julia*, *J. Open Res. Softw.* 5 (2017) 10.
- [38] Y. Nishihara (Ed.), *Applied Cross-Coupling Reactions, Lecture Notes in Chemistry*, vol. 80, Springer-Verlag, Berlin, Heidelberg, 2013.
- [39] T.E. Barder, S.D. Walker, J.R. Martinelli, S.L. Buchwald, Catalysts for Suzuki-Miyaura coupling processes: scope and studies of the effect of ligand structure, *J. Am. Chem. Soc.* 127 (2005) 4685–4696.
- [40] D.A. Conlon, B. Pipik, S. Ferdinand, C.R. LeBlond, J.R. Sowa, B. Izzo, P. Collins, G. Ho, J.M. Williams, Y. Shi, Y. Sun, Suzuki-Miyaura cross-coupling with quasi-heterogeneous palladium, *Adv. Synth. Catal.* 345 (2003) 931–935.
- [41] R. Narayanan, C. Tabor, M. El-Sayed, Can the observed changes in the size or shape of a colloidal nanocatalyst reveal the nanocatalysis mechanism type: Homogeneous or heterogeneous?, *Top Catal.* 48 (2008) 60–74.
- [42] J.D. Webb, S. MacQuarrie, K. McEleney, C.M. Crudden, Mesoporous silica-supported Pd catalysts: an investigation into structure, activity, leaching and heterogeneity, *J. Catal.* 252 (2007) 97–109.
- [43] S. Reimann, J. Stötzl, R. Frahm, W. Kleist, J.D. Grunwaldt, A. Baiker, Identification of the active species generated from supported Pd catalysts in Heck reactions: an in situ quick scanning EXAFS investigation, *J. Am. Chem. Soc.* 133 (2011) 3030–3921.
- [44] J.M. Richardson, C.W. Jones, Poly(4-vinylpyridine) and Quadrapure TU as selective poisons for soluble catalytic species in palladium-catalyzed coupling reactions - application to leaching from polymer-entrapped palladium, *Adv. Synth. Catal.* 348 (2006) 1207–1216.
- [45] A.F. Schmidt, A.A. Halaiqaa, V. Smirnov, Interplays between reactions within and without the catalytic cycle of the Heck reaction as a clue to the optimization of the synthetic protocol, *Synlett* 18 (2006) 2861–2878.